

Original citation:

Liang, Cunman, Wang, Fujun, Tian, Yanling, Zhao, Xingyu, Zhang, Hongjie, Cui, Liangyu, Zhang, Dawei and Ferreira, Placid. (2015) A novel monolithic piezoelectric actuated flexure-mechanism based wire clamp for microelectronic device packaging. Review of Scientific Instruments, 86 (4). 045106.

Permanent WRAP url:

<http://wrap.warwick.ac.uk/76447>

Copyright and reuse:

The Warwick Research Archive Portal (WRAP) makes this work by researchers of the University of Warwick available open access under the following conditions. Copyright © and all moral rights to the version of the paper presented here belong to the individual author(s) and/or other copyright owners. To the extent reasonable and practicable the material made available in WRAP has been checked for eligibility before being made available.

Copies of full items can be used for personal research or study, educational, or not-for profit purposes without prior permission or charge. Provided that the authors, title and full bibliographic details are credited, a hyperlink and/or URL is given for the original metadata page and the content is not changed in any way.

Publisher's statement:

Copyright (2015) American Institute of Physics. This article may be downloaded for personal use only. Any other use requires prior permission of the author and the American Institute of Physics.

A note on versions:

The version presented here may differ from the published version or, version of record, if you wish to cite this item you are advised to consult the publisher's version. Please see the 'permanent WRAP url' above for details on accessing the published version and note that access may require a subscription.

A novel monolithic piezoelectric actuated flexure-mechanism based wire clamp for microelectronic device packaging

Cunman Liang,¹⁾ Fujun Wang,^{1,a)} Yanling Tian,¹⁾ Xingyu Zhao,¹⁾ Hongjie Zhang¹⁾,
Liangyu Cui¹⁾, Dawei Zhang,¹⁾ and Placid Ferreira²⁾

¹⁾*Tianjin Key Laboratory of Equipment Design and Manufacturing Technology, School of Mechanical Engineering,
Tianjin University, Tianjin, 300072, China*

²⁾*Department of Mechanical Science and Engineering, University of Illinois at Urbana-Champaign, Urbana, 61801,
USA*

A novel monolithic piezoelectric actuated wire clamp is presented in this paper to achieve fast, accurate and robust microelectronic device packaging. The wire clamp has compact flexure-based mechanical structure and light weight. To obtain large and robust jaw displacements and ensure parallel jaw grasping, a two-stage amplification composed of a homothetic bridge type mechanism and parallelogram leverage mechanism was designed. Pseudo-rigid-body model (PRBM) and Lagrange approaches were employed to conduct the kinematic, static and dynamic modeling of the wire clamp, and optimization design was carried out. The displacement amplification ratio, maximum allowable stress and natural frequency were calculated. Finite element analysis (FEA) was conducted to evaluate the characteristics of the wire clamp and wire Electro Discharge Machining (EDM) technique was utilized to fabricate the monolithic structure. Experimental tests were carried out to investigate the performance, and the experimental results match well with the theoretical calculation and FEA. The amplification ratio of the clamp is 20.96, and the working mode frequency is 895 Hz. Step response test show the wire clamp has fast response and high accuracy, and the motion resolution is 0.2 μ m. High speed precision grasping operations of gold and copper wires were realized using the wire clasper.

I. INTRODUCTION

The microelectronic industry is a diverse industry that has grown tremendously over the past several decades. As one of the crucial microelectronic products, integrated circuits (ICs) have penetrated virtually all aspects of daily life¹⁻³. The demand for electronic products with high pin-count IC installations and high assembly density, such as scientific instruments, mobile phones, computers and cars, has been growing, which calls for high performance semiconductor interconnection technology between chips and packages^{4, 5}.

Thermosonic wire bonding achieves electrical interconnections between ICs and small pads on the lead frame/substrate using fine gold or other metal wires. It has been considered as the most cost-effective and flexible interconnecting technology for microelectronic device packaging and has been widely used within microelectronic packages of nearly any type⁶. Ever-increasing demands for higher productivity and better product quality in advanced semiconductor manufacturing industries

^{a)} Author to whom correspondence should be addressed. Electronic mail: wangfujun@tju.edu.cn

motivate the development of automatic wire bonding. A smaller pad size and finer pitch of semiconductor products require that high speed precision wire bonding equipment works in extreme conditions ⁷. As an important component of automatic wire bonders, wire clamps perform high-frequency open and close operations during wire bonding process (shown in Fig.1), and their characteristics have a significant influence on wire bonding performance ^{8, 9}. As a result, it is essential to design novel high-performance wire clamps to improve wire bonding efficiency and quality.

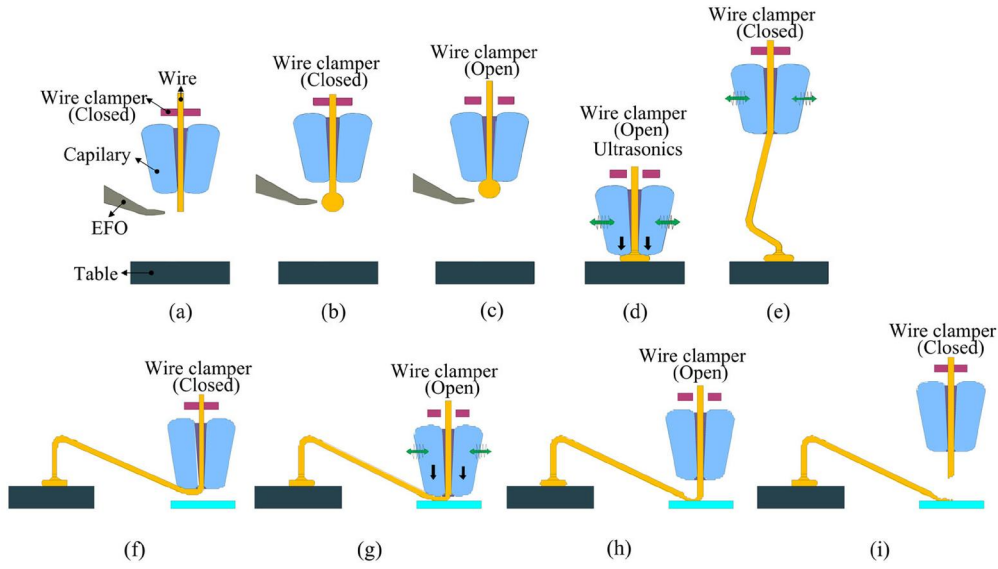


FIG. 1. The working process of thermosonic wire bonding.

The design of clamps with different specifications has received considerable attention from researchers ¹⁰. Most traditional wire clamps used for wire bonding adopt electromagnetic actuators as drivers ^{11, 12} and complex mechanisms as motion transmission parts. These kinds of clamps show appropriate performance. However, their applications in high speed wire bonding are limited due to a complex fabrication and assembly process as well as their poor anti-jamming characteristics ¹³. Electrostatic and electrothermal actuators have been used in microgrippers, but these grippers usually generate a very low grasping force, and thus are not suitable for wire bonding ¹⁴⁻¹⁶. Shape memory alloy actuators can produce large strokes. However, they can cycle only a few times before complete immobilization and have high fabrication costs, hysteresis, and short lifetime ¹⁷.

Piezoelectric (PZT) actuators have the advantages of high force output to weight ratio, fast response and zero backlash ¹⁸⁻²⁵, and thus they have been widely used in microgrippers. Chen et al. ²⁶ proposed a PZT driven flexure-based microgripper for optical fiber assembly. Zubir et al. ²⁷ developed novel hybrid flexure-based microgrippers for precision micro-object manipulation with an amplification ratio of 3.68 and a maximum jaw traveling range of 100μm. A novel driving principle

was presented by Huang et al.²⁸ by means of the parasitic motion of PZT actuated microgrippers. Although these microgrippers show appropriate performance, they are generally used for micro-object manipulation and assembly without considering high speed operations. As a result, they can not meet the stringent requirements of high speed precision wire bonding operations because vibrations can be generated during high frequency close and open motion, which will affect the bonding quality, even lead to bonding failures.

A novel monolithic piezoelectric actuated wire clamp is presented in this paper. A two-stage flexure-based amplification is designed, and a homothetic bridge type mechanism and parallelogram leverage mechanism are utilized to ensure high speed, parallel and robust jaw grasping. The kinematic, static and dynamic models of the wire clamp are established; then the clamp characteristics are analyzed using finite element analysis (FEA). The wire clamp is fabricated, and experimental tests are carried out to investigate its performance.

II. CONFIGURATION OF THE WIRE CLAMP

Figure 2 shows the mechanism of the piezoelectric actuated flexure-based wire clamp consisting of a stack piezoelectric ceramic actuator (SPCA), a pair of grasping jaws, a preload bolt, a base and a motion transmission mechanism designed as a two-stage amplification including a homothetic bridge type mechanism and a parallelogram leverage mechanism. As shown in Fig.2, the SPCA is connected with the motion transmission mechanism through the preload bolt at one end of the SPCA, and the preload force to the SPCA can be adjusted by the bolt. Both of the grasping jaws are fixed to the base, and the wire clamp is designed symmetrically along the longitudinal axis of the piezoelectric actuator to avoid shear force and bending torque acting on the SPCA.

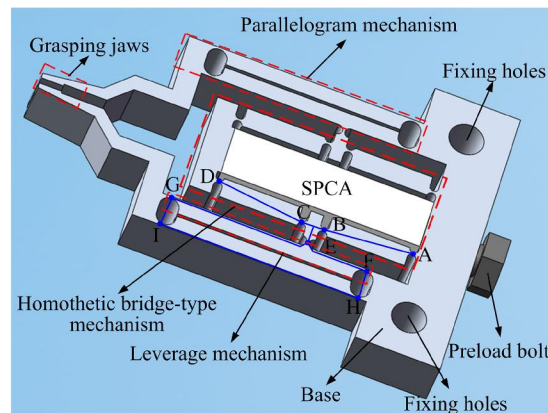


FIG. 2. The mechanism of the wire clamp.

The motion transmission is realized through the two-stage amplification. The homothetic bridge-type mechanism is composed of a connecting rod mechanism (A-B-C-D) based on double-notch circular flexure hinges, and its working principle is shown in Fig. 3(a). In order to obtain a large amplification ratio, a leverage mechanism (E-F-G) integrated within a parallelogram mechanism (F-G-H-I) at each side of the wire clamp was designed as the second-stage amplification connected by two flexure hinges of the connecting linkage. As shown in Fig. 3(b), pure jaw translations can be realized through the parallelogram mechanism, thus avoiding the sliding between the wire and jaws during grasping process, and more stable and firm wire grasping can be ensured due to the fact that the grasping force will act normal to the wires compared with the angular grasping mode²⁷. In order to grasp an object, a voltage should be applied to the SPCA to make it expand and push the homothetic bridge-type mechanism (A-B-C-D); then the homothetic bridge-type mechanism will pull the leverage mechanisms (E-F-G-H-I), causing the gripping jaws to close to grasp the manipulated wires. After power is switched off, the SPCA will retract to its initial position, and this causes the grasping jaws to open and release the manipulated wires.

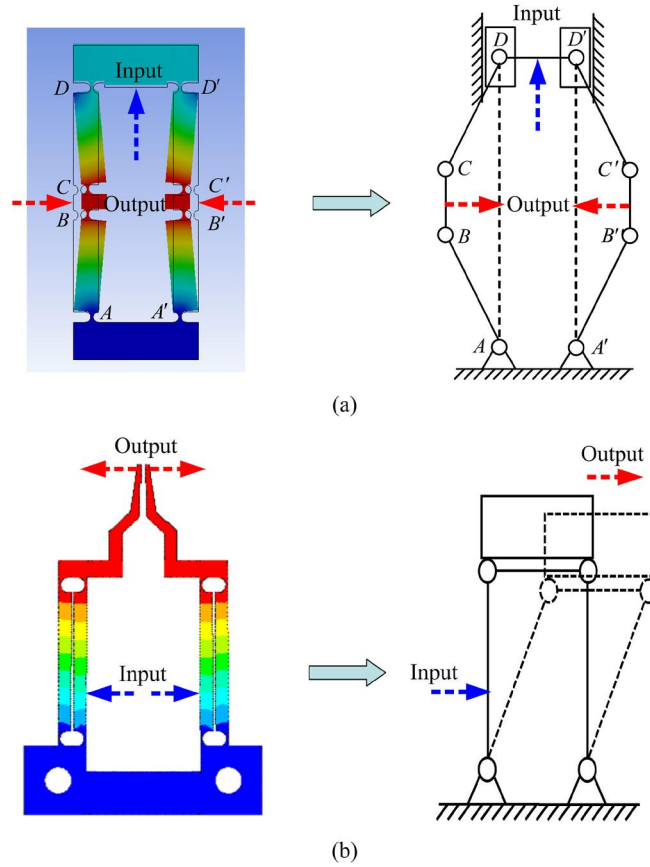


FIG. 3. The two-stage amplification: (a) the homothetic bridge-type mechanism; and (b) parallelogram mechanism.

III. MODELING AND DESIGN

A. Kinematic modeling

According to the Pseudo Rigid Body Model (PRBM) approach, the flexure hinges can be considered movable hinges with torsion springs while the drift of the rotational centers and the stiffness of flexure hinges are not taken into consideration and the links can be considered as rigid rods. As a result, the equivalent model of the piezoelectric actuated wire clamp is shown in Fig.4, where i ($i = A, B, \dots, I$) denotes the rotational centers of flexure hinges, and d_{in} and d_{out} are the input displacement from the SPCA and the output displacement of the grasping jaw, respectively.

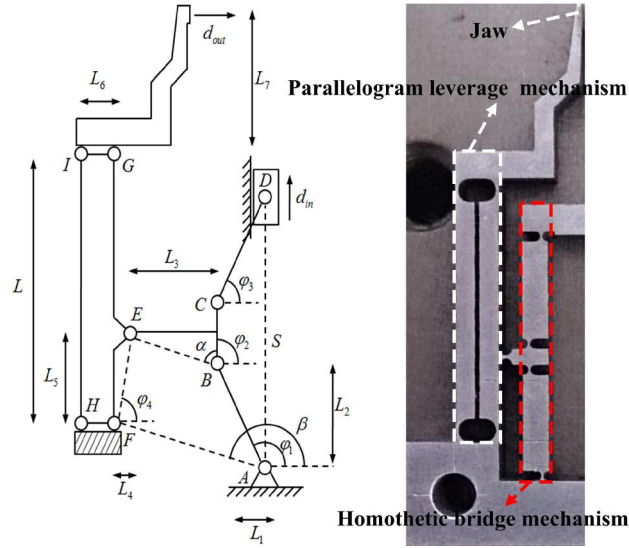


FIG. 4. Pseudorigid-body-model of the wire clamp.

As shown in Fig.4, A-B-C-D-E-F-G is equivalent to a six-bar linkage mechanism in which the linkages AB, BC, CD and FE have the initial angular positions of ϕ_1, ϕ_2, ϕ_3 , and ϕ_4 , respectively. The length of the linkages is L_i ($i=AB, BC, \dots, AF$). The angle α is the angle between linkages BC and BE, and the linkage AF has the angle β from the x-axis positive direction. The following equations are based on the geometric and motion relationships:

$$l_{AB}e^{i\phi_1} + l_{BE}e^{i(\phi_2+\alpha)} = l_{AF}e^{i\beta} + l_{FE}e^{i\phi_4} \quad (1)$$

$$l_{AB}e^{i\phi_1} + l_{BC}e^{i\phi_2} + l_{CD}e^{i\phi_3} = Se^{\frac{i\pi}{2}} \quad (2)$$

Differentiating Eqs (1) and (2) with respect to time yield

$$l_{AB}\omega_1e^{i(\phi_1+\frac{\pi}{2})} + l_{BE}\omega_2e^{i(\phi_2+\alpha+\frac{\pi}{2})} = l_{FE}\omega_4e^{i(\phi_4+\frac{\pi}{2})} \quad (3)$$

$$l_{AB}\omega_1 e^{i(\varphi_1 + \frac{\pi}{2})} + l_{BC}\omega_2 e^{i(\varphi_2 + \frac{\pi}{2})} + l_{CD}\omega_3 e^{i(\varphi_3 + \frac{\pi}{2})} = \dot{S}e^{i\frac{\pi}{2}} \quad (4)$$

where $\alpha = \arctan \frac{2l_3}{l_{BC}}$.

Let the real and imaginary parts be equal, respectively, and thus the following relationship can be written:

$$\omega_4 = b\omega_1 \quad (5)$$

$$\dot{S} = l_{AB}\omega_1 \cos \varphi_1 + l_{BC}\omega_2 \cos \varphi_2 + l_{CD}\omega_3 \cos \varphi_3 \quad (6)$$

where $a = -\frac{l_{AB} \sin(\varphi_1 - \varphi_4)}{l_{BE} \sin(\varphi_2 + \alpha - \varphi_4)}$, $b = \frac{l_{AB} \sin(\varphi_1 - \varphi_2 - \alpha)}{l_{EF} \sin(\varphi_4 - \varphi_2 - \alpha)}$, and $c = -\frac{l_{AB} \sin \varphi_1 + al_{BC} \sin \varphi_2}{l_{CD} \sin \varphi_3}$.

The displacement amplification ratio can be calculated as

$$R_{amp} = \frac{2\partial d_{out}}{\partial d_{in}} = 2 \frac{\partial d_{out} / \partial t}{\partial d_{in} / \partial t} = \frac{2v_G}{v_D} \quad (7)$$

where ∂d_{out} and ∂d_{in} are the small displacements of the single jaw and input end, respectively, v_D and v_G are the velocities of points D and G .

The velocities of points D and G can be written as

$$v_D = \frac{\partial d_{in}}{\partial t} = \dot{S} \quad (8)$$

$$v_G = \frac{\partial d_{out}}{\partial t} = \omega_4 L \quad (9)$$

Substituting Eq.(5), (6), (8) and (9) into Eq.(7), yields

$$R_{amp} = \frac{2bL}{l_{AB} \cos \varphi_1 + al_{BC} \cos \varphi_2 + cl_{CD} \cos \varphi_3} \quad (10)$$

B. Static modeling

When a small displacement d_{in} from the SPCA is applied to the input terminal of the wire clamp, the angle increments of each moving linkage can be obtained. Furthermore, the rotational angles of the flexure hinges can be calculated as

$$\psi_A = \frac{d_{in}}{\varepsilon} \quad (11)$$

$$\psi_B = \frac{ad_{in}}{\varepsilon} - \frac{d_{in}}{\varepsilon} = \frac{(a-1)d_{in}}{\varepsilon} \quad (12)$$

$$\psi_C = \frac{cd_{in}}{\varepsilon} - \frac{ad_{in}}{\varepsilon} - \frac{d_{in}}{\varepsilon} = \frac{(c-a-1)d_{in}}{\varepsilon} \quad (13)$$

$$\psi_D = \frac{d_{in}}{\varepsilon} + \frac{(a-1)d_{in}}{\varepsilon} + \frac{(c-a-1)d_{in}}{\varepsilon} = \frac{(c-1)d_{in}}{\varepsilon} \quad (14)$$

$$\psi_F = \frac{bd_{in}}{\varepsilon} \quad (15)$$

$$\psi_E = -\psi_A - \psi_B + \psi_F = \frac{(b-a)d_{in}}{\varepsilon} \quad (16)$$

where $\varepsilon = l_{AB} \cos \varphi_1 + al_{BC} \cos \varphi_2 + cl_{CD} \cos \varphi_3$, and the negative signs of the angles indicate that the rotational motion of the flexure hinge is in the clockwise direction.

Based on the PRBM approach, the static modeling of the wire clamp is performed to describe the force-deflection relationship of flexure hinges. The wire clamp is subsequently transformed into a rigid body mechanism by replacing the flexible segment with equivalent rigid joint and torsional spring. This approach will simplify the model to enable a conventional rigid body kinematic analysis to be performed for further investigation of the grasping performance and acquiring various critical design parameters.

The torsional spring constants of the flexural hinges can be estimated by

$$K_{r_i} = \begin{cases} \frac{2EBt_i^{5/2}}{9\pi r_i^{1/2}} & i = A, \dots, E \\ \frac{\sqrt{2}EBt_i^{5/2}}{9\pi r_i^{1/2}} & i = F, \dots, I \end{cases} \quad (17)$$

where r_i and t_i are the radius and thickness of the i th flexure hinge, respectively; E is the elastic modulus of the material, and B is the thickness of the wire clamp.

Since the flexure hinge in homothetic bridge-type mechanism should be the same to maintain symmetry, r_1 is defined as the radius of flexure hinges in the bridge-type mechanism; r_2 to be the radius of the flexure hinges in the connecting linkage, and r_3 to be the radius of the flexure hinges in the parallelogram mechanism.

Furthermore, the torque M_i , generated at the rotational center of the flexure hinges can be calculated by

$$M_i = -K_{r_i} \psi_i \quad i = A, \dots, I \quad (18)$$

where the negative sign indicates that the torque has the opposite direction with the rotational motion of the flexure hinge.

In order to derive the input stiffness of the wire clamp, the Castigliano's first theorem is adopted and expressed as

$$F_{in} = \frac{\partial U}{\partial d_{in}} \quad (19)$$

where d_{in} is the deformation due to the applied force, F_{in} is the applied force, and U is the deformation energy and given as

$$U = \frac{1}{2} \sum_{i=A}^I K_{ri} \psi_i^2 \quad (20)$$

Substituting Eqs(16)-(21) into Eq.(26), the following equation can be obtained:

$$U = \left[\frac{K_{rA} + K_{rB}(a-1)^2 + K_{rC}(c-a-1)^2}{K_{rD}(c-1)^2 + K_{rE}(b-a)^2 + 4K_{rF}b^2} + \right] \frac{d_{in}^2}{2\varepsilon^2} \quad (21)$$

The applied force can be expressed as

$$F_{in} = \frac{\partial U}{\partial d_{in}} = \left[\frac{K_{rA} + K_{rB}(a-1)^2 + K_{rC}(c-a-1)^2}{K_{rD}(c-1)^2 + K_{rE}(b-a)^2 + 4K_{rF}b^2} + \right] \frac{d_{in}}{\varepsilon^2} \quad (22)$$

The input stiffness of the wire clamp can be derived as

$$K_{in} = \frac{F_{in}}{d_{in}} = \frac{\left[K_{rA} + K_{rB}(a-1)^2 + K_{rC}(c-a-1)^2 + K_{rD}(c-1)^2 + K_{rE}(b-a)^2 + 4K_{rF}b^2 \right]}{\varepsilon^2} \quad (23)$$

Considering the PRBM of the wire clamp with external forces on the input terminal and jaw, and torques at each joint, the following equation can be obtained:

$$F_{in} = K_{in} d_{in} + \frac{R_{amp}}{2} F_{out} = \frac{2K_{in} d_{out}}{R_{amp}} + \frac{R_{amp}}{2} F_{out} \quad (24)$$

Eq. (30) describes the relationship among the output force, the input force, input displacement, output displacement, input stiffness and displacement amplification ratio of the wire clamp. It is known that the larger the displacement amplification ratio R_{amp} , the smaller the output force F_{out} . When the wire clamp does not grasp the wire, the output displacement is determined by the geometrical parameters of the wire clamp and the input force. When grasping the wire, the output displacement does not change when increasing the input force and the input displacement because the grasping jaws are fixed. Generally, the grasping jaws will close and then grasp the wire with increasing voltage applied to the wire clamp.

For further evaluation of the stress concentration at each flexure hinge, the reaction forces and torque of each flexure hinge should be determined as shown in Fig.5. Through the static equilibrium analysis of each rigid linkage, the following equations can be obtained:

$$F_{Ax} = F_{Bx} = F_{Cx} - F_{Ex} \quad (25)$$

$$F_{Ay} = F_{By} = F_{Cy} - F_{Ey} \quad (26)$$

$$F_{Dx} = -F_{Cx} = \frac{M_C + M_D - F_{Dy} L_1}{L_2} \quad (27)$$

$$F_{Dy} = -F_{Cy} = F_{in} \quad (28)$$

$$F_{Ex} = \frac{2(M_1 L_3 + M_2 L_4)}{2L_5 L_3 + L_{BC} L_4} \quad (29)$$

$$F_{Ey} = \frac{2M_3 L_5 - M_1 L_{BC}}{2L_3 L_5 + L_4 L_{BC}} \quad (30)$$

$$F_{Fx} = F_{Ex} - F_{Gx} \quad (31)$$

$$F_{Fy} = F_{Ey} - F_{Gy} \quad (32)$$

$$F_{Gx} = F_{Hx} = -F_{Ix} = -\frac{M_H + M_I}{L} \quad (33)$$

$$F_{Gy} = F_{Hy} = -F_{Iy} = \frac{M_G + M_I - F_{out} L_7}{L_6} \quad (34)$$

where $M_1 = M_E - M_F - M_G + F_{Gx} L$ and $M_2 = M_B + M_E - M_C + F_{Cx} L_{BC} / 2$.

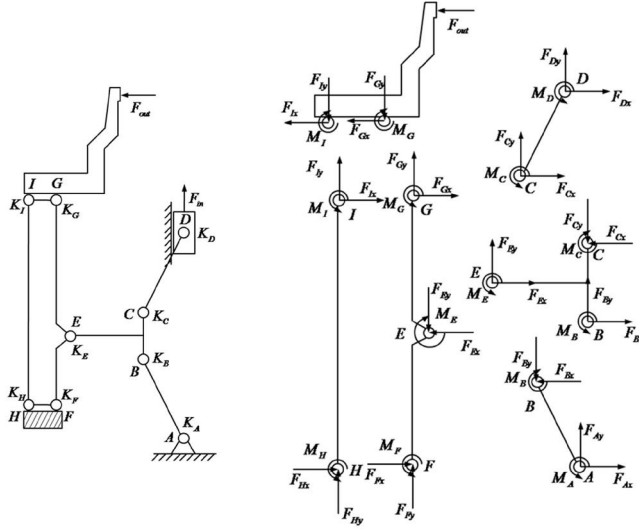


FIG. 5. Static force analysis.

For each flexure hinge, the maximum stress σ_{max} occurs at the outer surface of the thinnest part, and it can be expressed

as

$$(\sigma_{max})_i = \begin{cases} \left| \frac{4Et_i^{1/2}\psi_i}{3\pi r_i^{1/2}} + \frac{F_{iy}}{bt_i} \right| & i = A, B, C, D \\ \left| \frac{4Et_i^{1/2}\psi_i}{3\pi r_i^{1/2}} + \frac{F_{ix}}{bt_i} \right| & i = E \\ \left| \frac{2\sqrt{2}Et_i^{1/2}\psi_i}{3\pi r_i^{1/2}} + \frac{F_{iy}}{bt_i} \right| & i = F, G, H, I \end{cases} \quad (35)$$

The maximum allowable stress is considered. Thus

$$(\sigma_{\max})_i < \frac{[\sigma]}{n_a} \quad (36)$$

where $[\sigma]$ denotes the tensile yield stress and $n_a (n_a > 1)$ is the factor of safety.

C. Dynamic modeling

The natural frequencies can be derived by using the Lagrange's equation which can be expressed as

$$\frac{d}{dt} \left(\frac{\partial T}{\partial \dot{q}_i} \right) - \frac{\partial T}{\partial q_i} + \frac{\partial V}{\partial q_i} = F_i \quad i = 1, 2, \dots, n, \quad (37)$$

where T and V are the total kinetic energy and potential energy of the system, respectively, q_i is the generalized coordinate, n is the number of generalized coordinates and F_i represents the generalized nonconservative force.

The total kinetic energy of the system can be expressed as

$$T = \frac{1}{2} m_{in} \dot{x}_{in}^2 + I_{AB} \omega_1^2 + I_{CD} \omega_1^2 + (I_{FG} + I_{HI}) \omega_4^2 + m_{BCE} \dot{x}_E^2 + m_{out} \dot{x}_{out}^2 \quad (38)$$

where m_{in} is the mass of the input terminal of the wire clamp, m_{BCE} is the mass of the rigid frame BCE, m_{out} is the mass of the output terminal of the wire clamp, I_{AB} , I_{CD} , I_{EF} , I_{FG} and I_{HI} represent the moments of inertia of the linkages AB, CD, EF, FG and HI with respect to their corresponding instantaneous centers, respectively.

The total potential energy of the entire system is expressed as

$$V = \sum_{i=A}^I k_i \psi_i^2 \quad (39)$$

where k_i is the rotational stiffness of the flexure hinge i .

The dynamic model of the wire clamp can be expressed as

$$M \ddot{x}_{in} + K x_{in} = F \quad (40)$$

$$\text{where } M = m_{in} + \frac{2(I_{AB} + I_{CD})}{\varepsilon^2} + \frac{2b^2(I_{FG} + I_{HI})}{\varepsilon^2} + \frac{2m_{BCE}L_{EF}^2}{\varepsilon^2} + 2m_{out}R_{amp}^2,$$

$$K = 2 \left(\frac{K_{rA}}{\varepsilon^2} + \frac{K_{rB}(a-1)^2}{\varepsilon^2} + \frac{K_{rC}(c-a-1)^2}{\varepsilon^2} + \frac{K_{rD}(c-1)^2}{\varepsilon^2} + \frac{K_{rE}(b-a)^2}{\varepsilon^2} + \frac{4K_{rF}b^2}{\varepsilon^2} \right), \text{ and } F = 2F_{in} - R_{amp}F_{out}.$$

The natural frequencies can be calculated as

$$f_1 = \frac{1}{2\pi} \sqrt{\frac{K}{M}} \quad (41)$$

D. Optimization design

Optimization design is carried out. The working mode frequency is chosen as the optimization objective function, and the input stiffness and the maximum stress are the constraints. The optimization work is concluded as follows:

- 1) Objective: Maximize the working mode frequency (f_1).
- 2) Related parameters: t , r_1 , r_2 and r_3 .
- 3) Subject to:
 - a) Input stiffness: $K_{in} \leq 20\%k_{SPCA}$;
 - b) Maximum stress: Eq. (36), and $n_a=2$;
 - c) Parameter ranges: $0.2\text{mm} \leq t \leq 0.5\text{mm}$, $0.3\text{mm} \leq r_1 \leq 1\text{mm}$, $0.5\text{mm} \leq r_2 \leq 1\text{mm}$, and $0.5\text{mm} \leq r_3 \leq 1\text{mm}$.

Using MATLAB optimization toolbox with the initial values $x = [t, r_1, r_2, r_3] = [0.3, 0.5, 0.8, 0.8]$, the optimization result is obtained as follows: $t=0.2\text{mm}$, $r_1=0.4\text{mm}$, $r_2=0.5\text{mm}$, $r_3=0.9\text{mm}$, $R_{amp}=21.7$, $k_{in}=7.5\text{N}/\mu\text{m}$, $\sigma_{max}=186\text{MPa}$ and the working mode frequency $f_1=914\text{Hz}$.

IV. CHARACTERISTIC ANALYSIS

The characteristics of the wire clamp were investigated using FEA, and the finite element model was established with the aid of ANSYS software to investigate the displacements of the jaw as well as flexure hinges and moving linkages, maximum stress concentration, and dynamic performance, etc. The actuation displacement was applied by the SPCA on the input terminal of the wire clamp. The deformation behavior of the jaw as well as flexure hinges and moving linkages under the input displacement of $10\mu\text{m}$ applied by the SPCA is shown in Fig.6. The maximum displacement of a jaw can reach $97\mu\text{m}$ which can enable firm and robust grasping operations with a large range of wires. Thus the displacement amplification ratio of one gripping jaw is 19.4. The displacement amplification ratio by FEA is smaller than the mathematical amplification ratio of 21.7, mainly because of the “displacement loss” effect arising from the combination of lever arm bending and connection flexure stretching which causes the actual lever amplification ratio to be smaller than the ideal value. FEA result shows that the maximum stress generated at the flexure hinge D is 192MPa , and it is far less than the yield strength (503MPa) of the material. Figure 7 depicts the range of grasping clearances for the clamp’s jaws by FEA.

Modal analysis is a very effective method to examine the dynamic performance of the wire clamp. Through modal analysis, the first four natural frequencies and corresponding mode shapes were obtained and shown in Fig.8. The first mode shape of the wire clamp is that the jaws and the parallelogram mechanism vibrate in the same direction and the corresponding natural frequency is 672 Hz . The second mode shape shows the jaws vibrate in the opposite directions and the corresponding natural frequency is 920 Hz . In the third mode shape the beam of the homothetic bridge-type mechanism swings along the horizontal direction and the corresponding natural frequency is 1676 Hz . Fig.6(d) describes the forth mode shape, in which

the vibration is generated from the first stage amplifications, via the second stage amplifications and finally transferred to the third amplifications and the jaws, and the corresponding natural frequency is 1805 Hz.

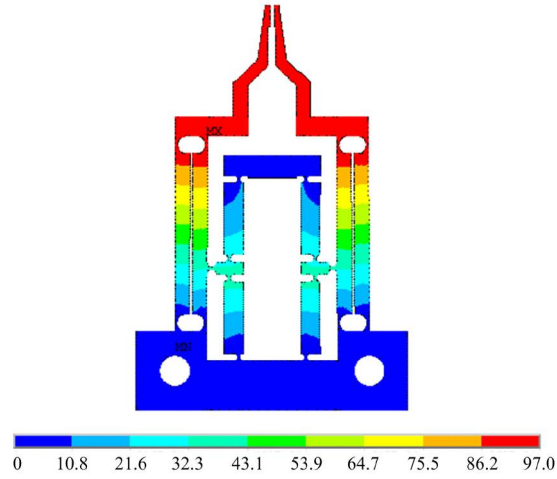


FIG. 6. Static analysis result by FEA..

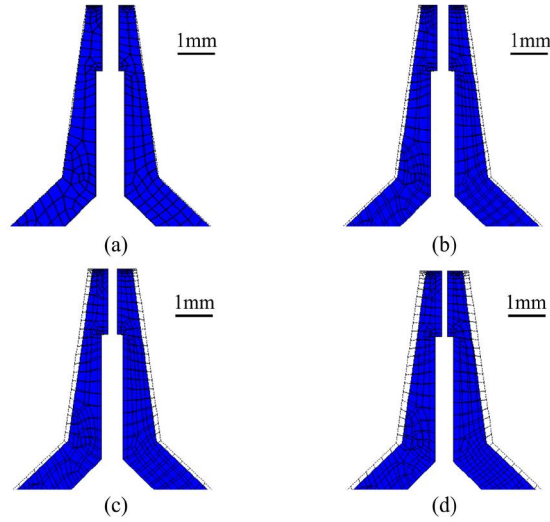


FIG. 7. Deformation behavior of the wire clamp with different grasping clearances for the clamp's jaws by FEA. (a) 400 μ m, (b) 300 μ m, (c) 200 μ m and (d) 100 μ m.

V. EXPERIMENTS

Figure 9 shows the prototype of the wire clamp actuated by a stack piezoelectric ceramic actuator (SPCA) (type: XP 5 \times 5/18, output displacement: 0–18 μ m, applied voltage: 0–150V, maximum driving force: 1400N). The wire clamp was fabricated through wire electro-discharge machining (wire EDM) technique to guarantee the geometrical accuracy of the

crucial sections of the clamp, and it was made from the material of AL7075-T651, which has the property of high elasticity, yield strength and light mass.

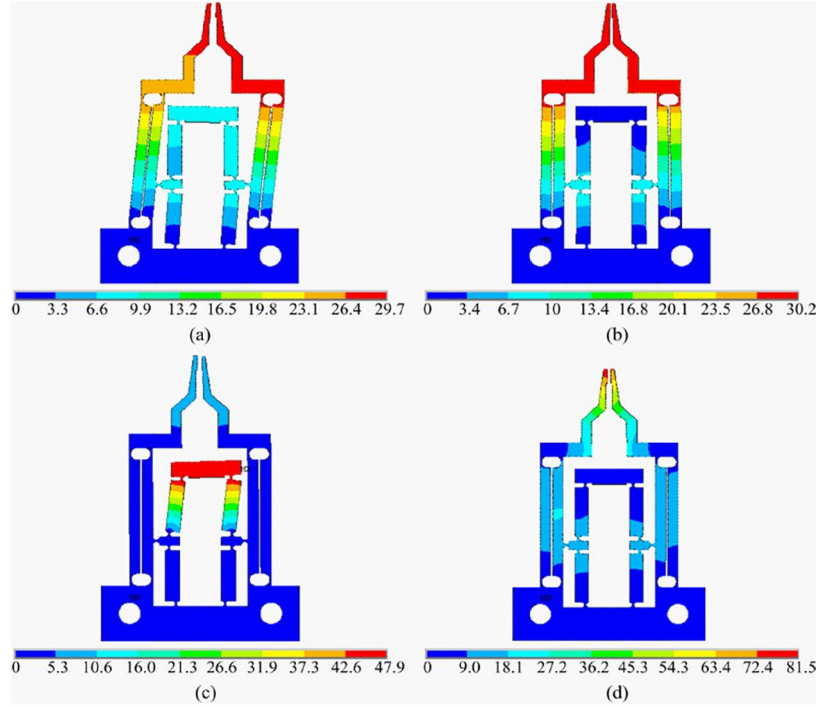


FIG. 8. First four mode shapes of the wire clamp.

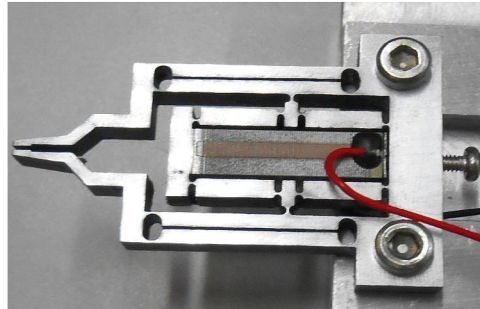


FIG. 9. The prototype of the wire clamp.

The wire clamp performance was investigated, and the experimental setup is displayed in Fig. 10, which is mainly composed of the developed wire clamp, laser displacement sensors (LK-H050 from Keyence, Inc) and the voltage control unit including the PI voltage amplifier, dSPACE DS1103 controller and universal interface, and the computer. All the devices were placed on a vibration-isolated Newport RS-4000 table. The basic operation of the system was carried out by applying the desired voltage from the voltage control unit to the SPCA to activate the output motion at the tip of the wire clamp. By changing the driving voltage the stable operations were offered to implement continuous expansion and retraction motions.

The wire clamp was preloaded through tightening the preloaded bolt against the base, and the initial clearance of the jaws was pre-adjusted as 400 μm . The grasping behavior of the wire clamp was observed with the aid of a microscope with a super depth 3D analysis system (VHX-1000 from Keyence, Inc), and the variable clearances of the grasping jaws during grasping motion are shown in Fig. 11.

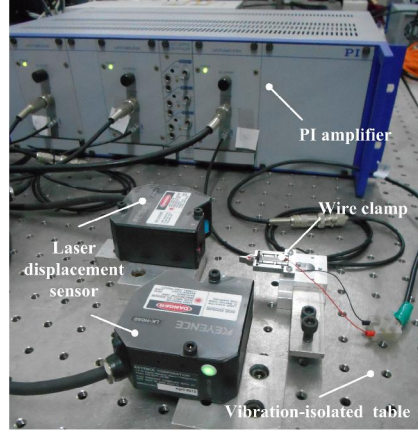


FIG. 10. Experimental setup.

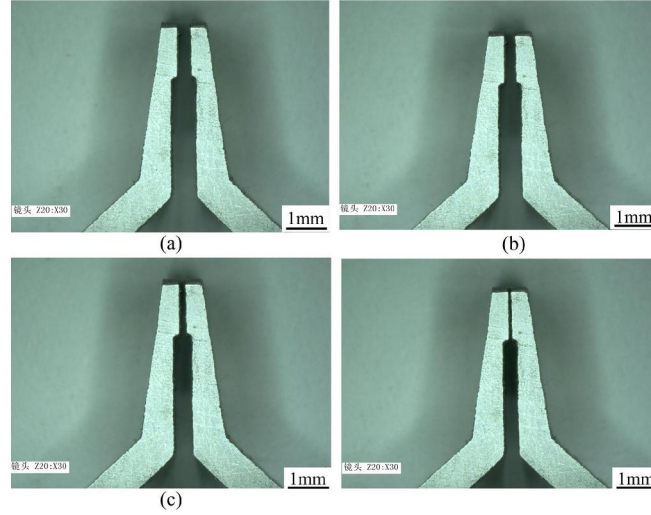


FIG. 11. Variable grasping clearances for the wire clamp's jaws by experiments. (a) 400 μm , (b) 300 μm , (c) 200 μm and (d) 100 μm .

Experiments were carried out to evaluate the grasping capacity of the wire clamp through grasping a gold wire with a diameter of 25.4 μm and a copper wire with a diameter of 100 μm . The grasping process was captured by a super depth 3D analysis system (VHX-1000 from Keyence, Inc) with a high pixel resolution, and Figs.12 and 13 provide the grasping process of the gold wire and copper wire, respectively.

Figure 14 summarizes the tip displacement of one grasping jaw of the wire clamp varying with the input displacement obtained by different approaches. Fig. 14 shows that the experimental measured displacement amplification ratio is 10.48 for one gripping jaw, which is in good agreement with the results by mathematical modeling and FEA, so the total displacement amplification ratio of the wire clamp is 20.96.

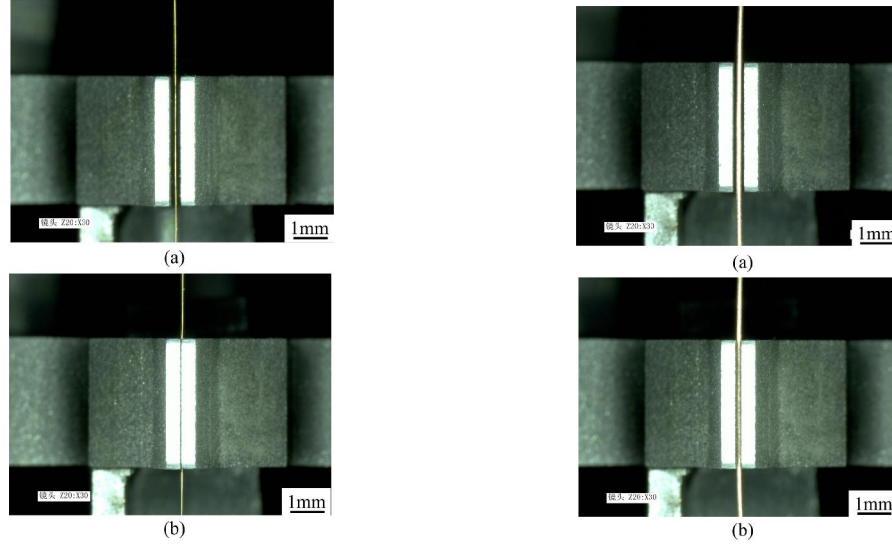


FIG. 12. Grasping a gold wire. (a) before grasping, and (b) after grasping. FIG. 13. Grasping a copper wire. (a) before grasping, and (b) after grasping.

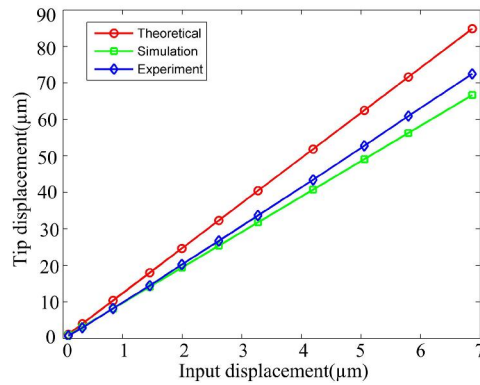


FIG. 14. Relationship between the tip displacement of a single jaw and the input displacement.

The vibration frequency of the fabricated wire clamp was tested by applying a swept sine signal to the SPCA. In the experiment, the wire clamp was driven by a voltage with amplitude of 20V and a frequency from 0.01 to 1500Hz. The vibrations of the wire clamp were observed with the aid of the Keyence VHX-1000 microscope. The dynamic response of the wire clamp is shown in Fig.15, and the result shows that the working mode frequency is 895Hz and the first local vibration model obtained by FEA was not excited.

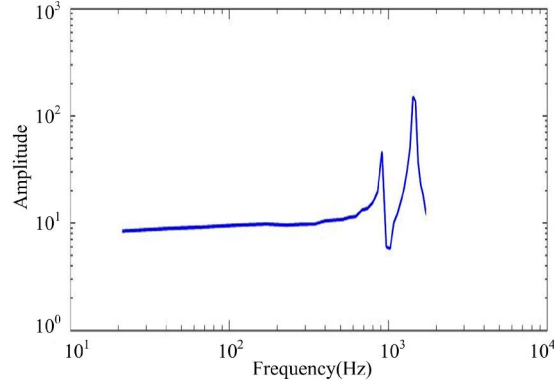


FIG. 15. Dynamic measurement result..

The step response of the wire clamp was investigated. A step voltage with amplitude of 10V is utilized to actuate the wire clamp, and the displacement response was recorded and shown in Fig.16. The overshoot of the motion is $1.3\mu\text{m}$, the displacement steady-state error is $0.2\mu\text{m}$, and the setting time is 21ms. The result shows that the wire clamp provides for good performance, and high speed precision grasping operations can be realized using the wire clasper.

The resolution of motion system is the minimal displacement of system steady-state motion. Reducing the motion increments gradually, the resolution of the system can be obtained through observing the minimal displacement value from the system is in steady state motion. From Fig. 17, it can be seen that the resolution is $0.2\mu\text{m}$.

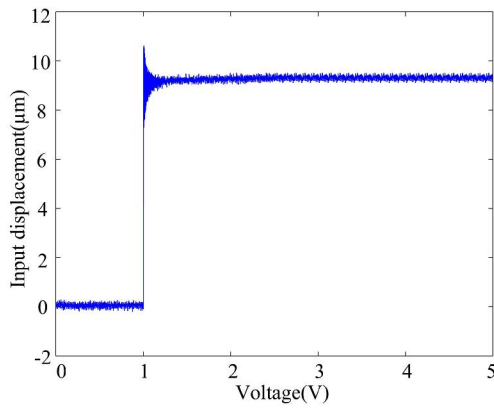


FIG. 16. Step response of the wire clamp.

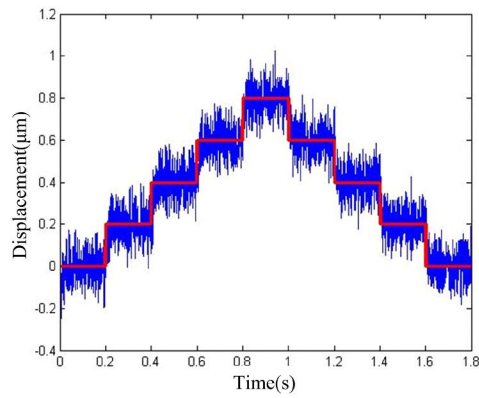


FIG. 17. Motion resolution of the wire clamp.

VI. CONCLUSION

The mechanism, modeling, characteristic analysis, fabrication and experimental test of a novel piezoelectric actuated wire clamp have been reported in this paper. A large displacement amplification ratio has been achieved through a two-stage

flexure-based amplification and parallel jaw grasping has been realized. By use of the PRBM and Lagrange approaches the kinematic, static, and dynamic models have been established. The characteristics of the wire clamp have been analyzed using FEA and it has been manufactured through wire EDM technique. Experimental tests have been implemented to examine the performance of the wire clamp, and the results show that the amplification ratio of the developed wire clamp is 20.96, and the working mode frequency is 895 Hz. The wire clamp has successfully grasped gold and copper wires. The step response and motion resolution of the wire clamp has been investigated, and the results indicate that the wire clamp provides for good performance and high speed precision grasping operations can be realized using the wire clasper.

ACKNOWLEDGMENTS

The supports of this work by the National Natural Science Foundation of China (Grant no. 51205279, 51275337 and 51175372), and the Science & Technology Commission of Tianjin Municipality (Grant no. 13JCQNJC04100), the Tianjin University for Peiyang Elite Scholar (Grant no. 60301014) and CSC Scholarship are gratefully acknowledged.

REFERENCES

- [1] M. Lofrano, B. Vandevelde, M. Gonzalez, A multilevel sub-modeling approach to evaluate 3D IC packaging induced stress on hybrid interconnect structures, *Microelectronic Engineering*, 2014, 120: 85-89.
- [2] W. Yao, C. Basaran, Electric pulse induced impedance and material degradation in IC chip packaging, *Electronic Materials Letters*, 2013, 9(5): 565-568.
- [3] H. Zhang, F. Wang, X. Zhao, D. Zhang, Y. Tian, Electrical matching of a piezoelectric ultrasonic transducer for microelectronic bonding, *Sensors and Actuators A: Physical*, 2013: 199(1): 241-249.
- [4] K. Wei, M. Du, L. Xie, Study of bonding wire failure effects on external measurable signals of IGBT module, *IEEE Transactions on Device and Materials Reliability*, 2014, 14(1): 83-89.
- [5] F. Wang, J. Li, S. Liu, X. Zhao, D. Zhang, Y. Tian, An improved adaptive genetic algorithm for image segmentation and vision alignment used in microelectronic bonding, *IEEE/ASME Transactions on Mechatronics*, 2014, 19(3): 916-923.
- [6] F. Wang, X. Zhao, D. Zhang, Z. Ma, X. Jing, Robust and precision control for a directly driven XY table, *Proceedings of IMechE, Part C, Journal of Mechanical Engineering Science*, 2011, 225(5): 1107-1120.
- [7] Z.Z. Liu, F.L. Luo, M.A. Rahman, Robust and precision motion control system of linear-motor direct drive for high-speed X-Y table positioning mechanism. *IEEE Trans. Ind. Electron.*, 2005, 52(5), 1357-1363.
- [8] H. Seppänen, R. Kurppa, A. Meriläinen, E. Häggström, Real time contact resistance measurement to determine when microwelds start to form during ultrasonic wire bonding, *Microelectronic Engineering*, 2013, 104: 114-119.

- [9] W. Feng, Q. Meng, Y. Xie, H. Fan, Wire bonding quality monitoring via refining process of electrical signal from ultrasonic generator, *Mechanical Systems and Signal Processing*, 2011, 25: 884-900.
- [10] F. Wang, C. Liang, Y. Tian, X. Zhao, and D. Zhang, Design of a piezoelectric-actuated microgripper with a three-stage flexurebased amplification, *IEEE/ASME Transactions on Mechatronics*, DOI:10.1109/TMECH.2014.2368789, 2014.
- [11] D.M. Dozor, Magnetostrictive wire bonding clamp for semiconductor packaging: Initial prototype design, modeling, and experiments, *Proceedings of SPIE - Industrial and Commercial Applications of Smart Structures Technologies*, CA, USA, 1998, 3326: 516-526.
- [12] D.K. Fan, F.L. Wang, Finite element analysis of wire clamp for wire bonding, *Proceedings of International Conference on Electronic Packaging Technology & High Density Packaging*, Guilin, China, 2012: 955-958.
- [13] Z. Long, L. Zhang, J. Zhang, FEM design and experiment of a micro-gripper based on piezoelectric material, *Advanced Materials Research*, 2012, 479-481: 434-438.
- [14] F. Beyeler, A. Neild, S. Oberti, D. J. Bell, Y. Sun, J. Dual, B.J. Nelson, Monolithically fabricated microgripper with integrated force sensor for manipulating microobjects and biological cells aligned in an ultrasonic field, *Journal of Microelectromechanical System*, 2007, 16(1): 7-15.
- [15] T. Chen, L. Chen, L. Sun, X. Li, Design and fabrication of a four-arm-structure MEMS gripper, *IEEE/ASME Trans. Electronics*, 2009, 56(4): 996-1003.
- [16] N. Chronis, L.P. Lee, Electrothermally activated SU-8 microgripper for single cell manipulation in solution, *Journal of Microelectromechanical Systems*, 2005, 14(4): 857-862.
- [17] M. Kohl, E. Just, W. Pfleging, S. Miyazaki, SMA microgripper with integrated antagonism, *Sens. Actuators A-Phys.*, 2000, A83(1-3): 208-213.
- [18] H. Tang, Y. Li, Development and active disturbance rejection control of a compliant micro/nano-positioning piezo-stage with dua-mode, *IEEE Transactions on Industrial Electronics*, 2014, 61(3): 1475-1492.
- [19] Y. Tian, B. Shirinzadeh, D. Zhang, Design and dynamics of a 3-DOF flexure-based parallel mechanism for micro/nano manipulation, *Microelectronic Engineering*, 2010, 87: 230-241.
- [20] Z. Wu, Y. Li, Design, Modeling, and analysis of a novel microgripper based on flexure hinges, *Advances in Mechanical Engineering*, 2014, 947584: 1-11.
- [21] G. Gu, L. Zhu, C. Su, Modeling and compensation of asymmetric hysteresis nonlinearity for piezoceramic actuators with amodified Prandtl- Ishlinskii model, *IEEE Transactions on Industrial Electronics*, 2014, 61(3): 1583–1595.

- [22] G. Gu, M. Yang, L. Zhu, Real-time inverse hysteresis compensation of piezoelectric actuators with a modified Prandtl-Ishlinskii model, *Review of Scientific Instruments*, 2012, 83(6): 065106.
- [23] Q. Xu, Design and testing of a novel multi-stroke micropositioning system with variable resolutions, *Review of Scientific Instruments*, 2014, 85(2): 025002.
- [24] Y. Qin, Y. Tian, D. Zhang, B. Shirinzadeh, S. Fatikow, A novel direct inverse modeling approach for hysteresis compensation of piezoelectric actuator in feedforward applications, *IEEE/ASME Transactions on Mechatronics*, 2013, 18(3): 981-989.
- [25] Z. Wu, Y. Li, Design, modeling and analysis of a novel micro-gripper based on flexure hinges, *Advances in Mechanical Engineering*, 2014, 947584: 1-11.
- [26] W.H. Chen, X.H. Shi, W.J. Chen, J.B. Zhang, A two degree of freedom micro-gripper with grasping and rotating functions for optical fibers assembling, *Review of Scientific Instruments*, 2013, 84(11): 115111.
- [27] M.N.M. Zubir, B. Shirinzadeh, Y.L. Tian, Development of a novel flexure-based microgripper for high precision micro-object manipulation, *Review of Scientific Instruments*, 2009, 80(6): 065106.
- [28] H. Huang, H.W. Zhao, Z.J. Yang, J. Mi, A novel driving principle by means of the parasitic motion of the microgripper and its preliminary application in the design of the linear actuator, *Review of Scientific Instruments*, 2012, 83(5): 055002.